Electronic Supplementary Material (ESI) for Journal of Materials Chemistry C.

Supporting Information

Stable dye-encapsulated indium−organic framework as dual-emitting sensor for the detection of Hg^{2+}/$Cr_2O_7^{2-}$ and a wide range of nitro-compounds

Hong-Ru Fu,[a] Ying Zhao,[a] Tao Xie,[a] Min-Le Han,[a] Lu-Fang Ma*[a,b] and Shuang-Quan Zang[b]

[a]*College of Chemistry and Chemical Engineering, Henan Province Function-oriented Porous Materials Key Laboratory, Luoyang Normal University, Luoyang, 471934 Henan, P. R. China.*

[b]*College of Chemistry and Molecular Engineering, Zhengzhou University, Zhengzhou, 450001 Henan, P. R. China.*

* Corresponding Author

Email: mazhuxp@126.com

1. Materials and measurements

All solvents and reagents were commercially available and used without further purification. Powder X-ray diffraction (PXRD) were measured on a D/Max-2500 diffractometer using Cu-*K*α (λ = 1.5418 Å) beam at room temperature. Thermogravimetric analyses (TGA) were conducted on a Netszch TGA 209 F3 thermogravimeter with a heating rate of 5 °C min^{-1} in air atmosphere. Elemental analyses for C, H, and N were performed on a PerkinElmer 240 microelemental analyzer. UV−vis spectra were obtained with a UV-2600 spectrophotometer in the range of 250−800 nm at room temperature. The solid UV−vis adsorption was performed on a Shimadzu UV-2450 spectrophotometer. Room-temperature emission and excitation spectra for the samples were recorded by a Hitachi F7000 fluorescence spectrometer. The surface area was measured on a Micromeritics ASAP 2020 at 77 K under liquid nitrogen. In order to remove guests, the crystal sample of compound 1 was activated with ethanol 10 times in three day, and then treated at 333 K under high vacuum for 20 h. The pore and surface area characterizatio of **1⊃DSM** is similar to that of compound **1**.

2. The structure of compound 1

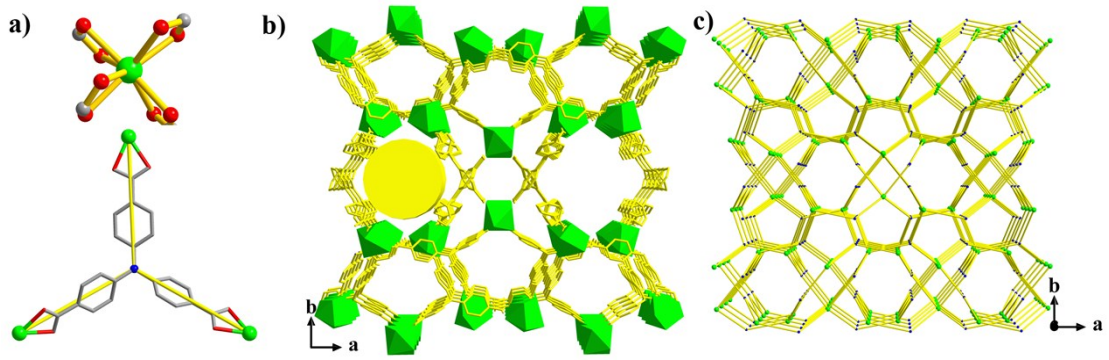

Figure S1. (a) The coordination environment of compound **1**; (b) 3D framework of compound **1** along the c axis; (b) 3D topological structure of compound **1** along the c axis.

3. The encapsulation of dye

The anion exchange capacity of compound **1** were evaluated by measuring the decolorization rate of aqueous DSM solution, which was calculated by the following formula:

$$q_e = \frac{(C_i - C_e)V}{W}$$

where C_i and C_e (mg g^{-1}) are the initial and equilibrium DSM concentration, respectively. V (mL) is the volume of DSM solution, W(mg) is the mass of adsorbent. After exchange, the solid samples were centrifuged, rinsed with water and dried in the air, namely **1⊃DSM**. The C_i was obtained Beer–Lambert law through UV-vis absorption spectra.

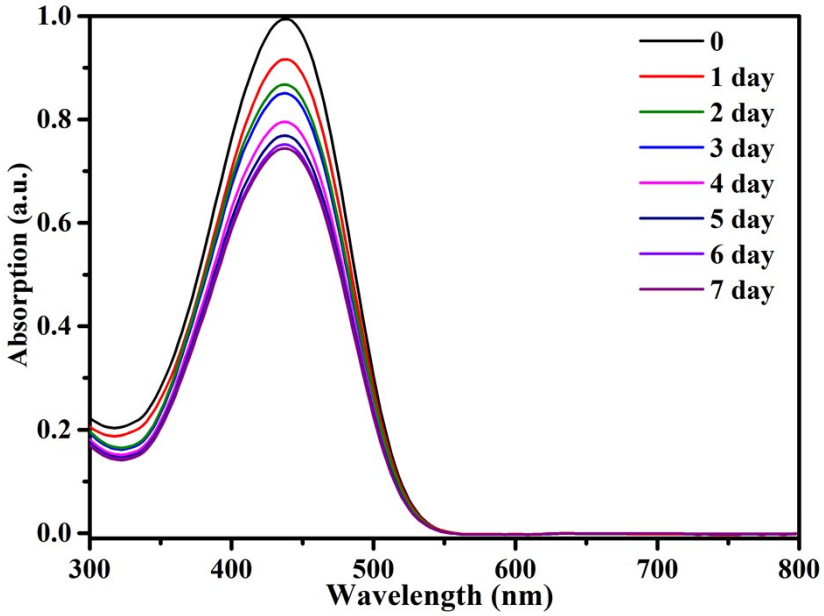

Figure S2. UV-vis absorption spectra of DSM solution during the ion-exchange process

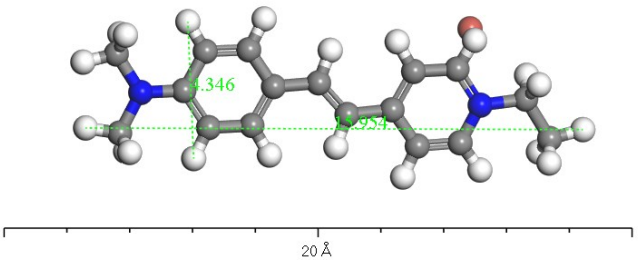

Figure S3. The size of DSM calculated by Materials Studio 7.0 system.

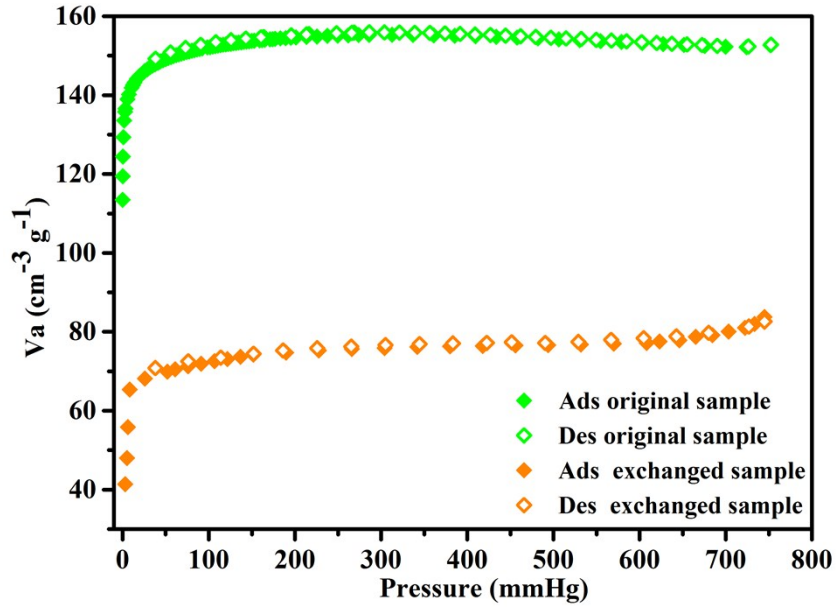

Figure S4. The N_2 adsorption of compound **1** before and after DSM adsorption.

4. The sensing testings

4.1 The sensing of inorganic ions in aqueous solution

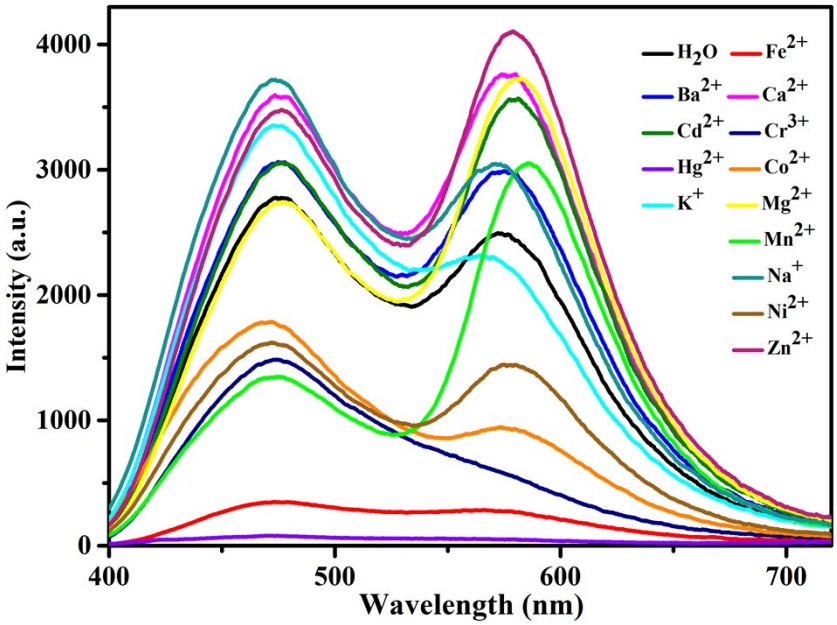

Figure S5. The luminescent intensity of **1⊃DSM** in the aqueous solution of various anion ions, the concentration for each ion is 1×10^{-3} mol L^{-1}.

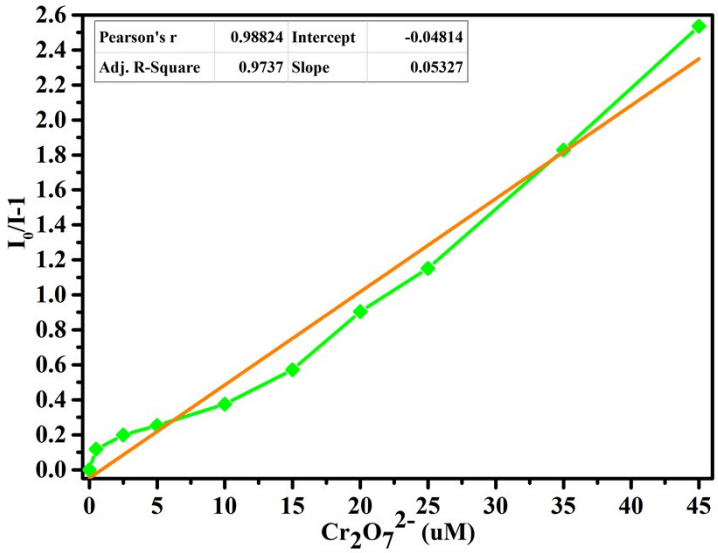

Figure S6. Plot showing the quenching ratio of luminescent intensity of **1⊃DSM** towards $Cr_2O_7^{2-}$; the data points in the low concentration range from 0 to 75 μM is fitted in a linear relationship.

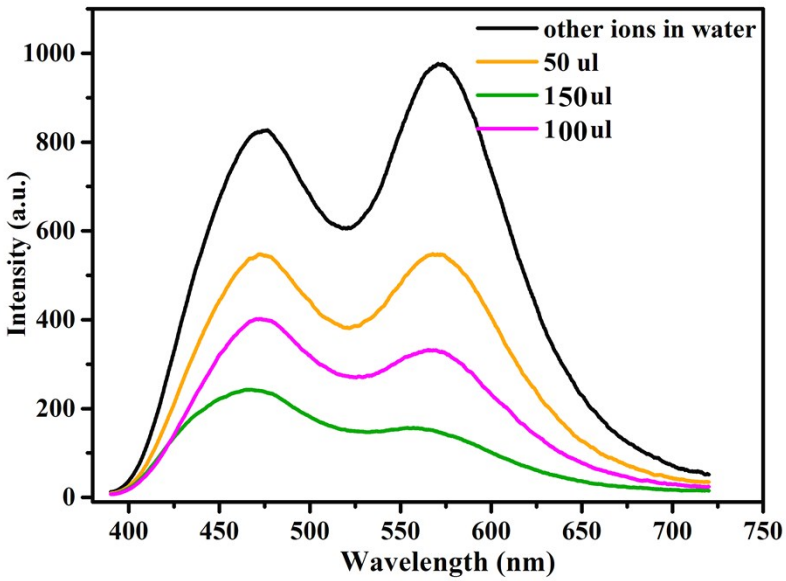

Figure S7. Competitive tests of **1⊃DSM** against $Cr_2O_7^{2-}$ (The concentration of other anions is 1×10^{-4} mol L^{-1}). black line: the luminescent intensity of **1⊃DSM** in aqueous solution of other anions. Orange, pink and green lines indicate that 50, 100 and 150 μL, 1×10^{-3} mol L^{-1} $Cr_2O_7^{2-}$ solution was added into the solution. (Orange, pink and green lines indicate that 50, 100 and 150 μL $Cr_2O_7^{2-}$ (1×10^{-3} mol L^{-1}) was added into the solution, respectively.

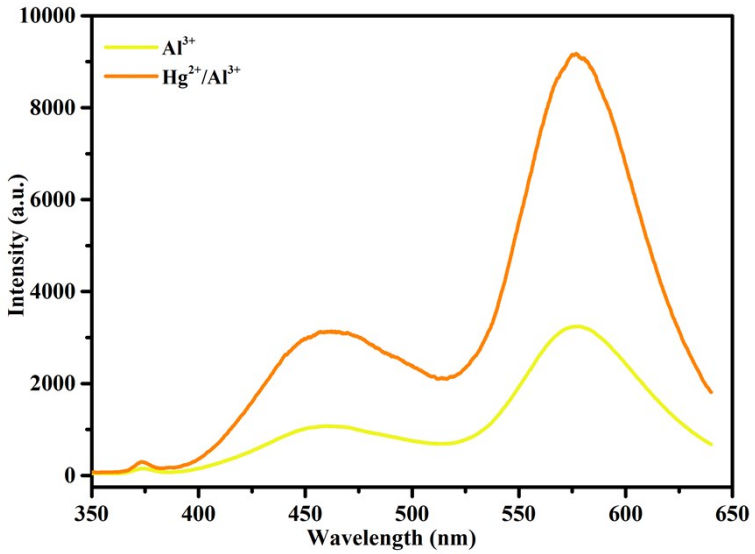

Figure S8. Luminescence intensity comparison of **1⊃DSM** upon addition of Hg^{2+} in the aqueous solution of Al^{3+} ion. The concentration of Hg^{2+} and Al^{3+} ions is 1×10^{-3} and 5×10^{-2} mol L^{-1}.

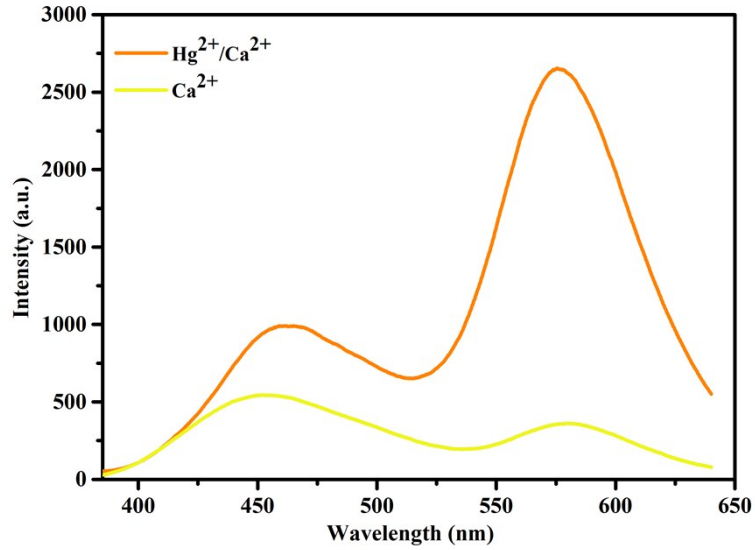

Figure S9. Luminescence intensity comparison of **1⊃DSM** upon addition of Hg^{2+} in the aqueous solution of Ca^{2+} ion. The concentration of Hg^{2+} and Ca^{2+} ions is 1×10^{-3} and 5×10^{-2} mol L^{-1}.

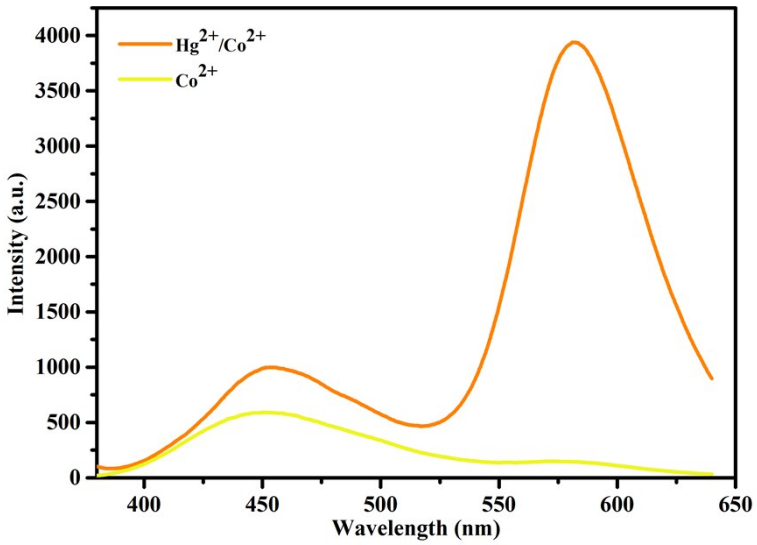

Figure S10. Luminescence intensity comparison of **1⊃DSM** upon addition of Hg^{2+} in the aqueous solution of Co^{2+} ion. The concentration of Hg^{2+} and Co^{2+} ions is 1×10^{-3} and 5×10^{-2} mol L^{-1}.

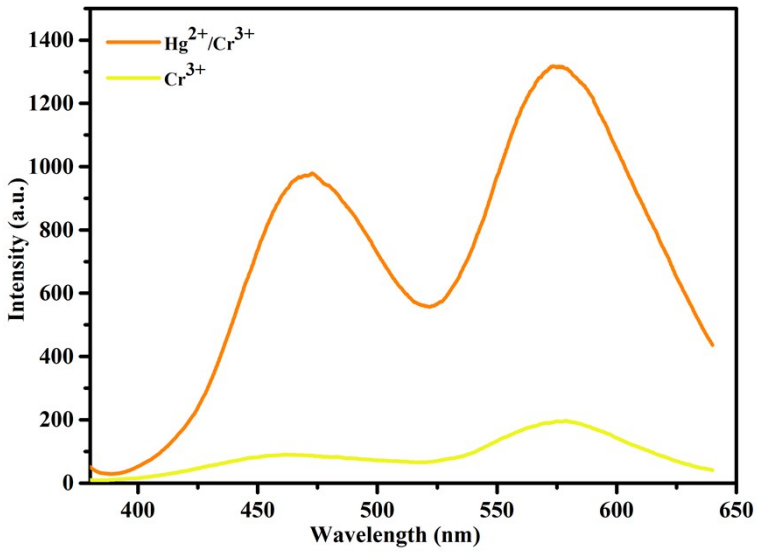

Figure S11. Luminescence intensity comparison of **1⊃DSM** upon addition of Hg^{2+} in the aqueous solution of Cr^{3+} ion. The concentration of Hg^{2+} and Cr^{3+} ions is 1×10^{-3} and 5×10^{-2} mol L^{-1}.

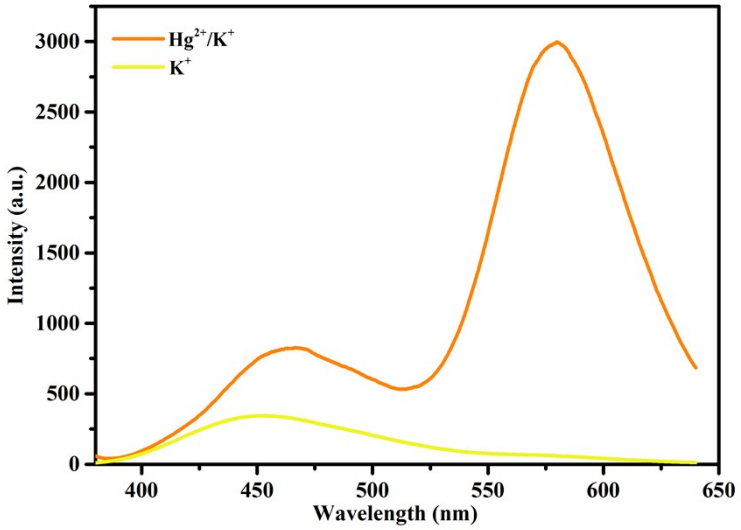

Figure S12. Luminescence intensity comparison of **1⊃DSM** upon addition of Hg^{2+} in the aqueous solution of K^+ ion. The concentration of Hg^{2+} and K^+ ions is 1×10^{-3} and 5×10^{-2} mol L^{-1}.

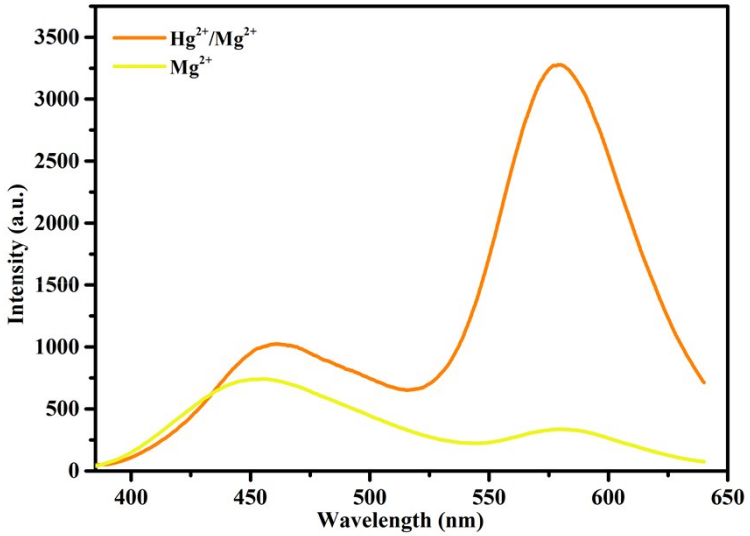

Figure S13. Luminescence intensity comparison of **1⊃DSM** upon addition of Hg^{2+} in the aqueous solution of Mg^{2+} ion. The concentration of Hg^{2+} and Mg^{2+} ions is 1×10^{-3} and 5×10^{-2} mol L^{-1}.

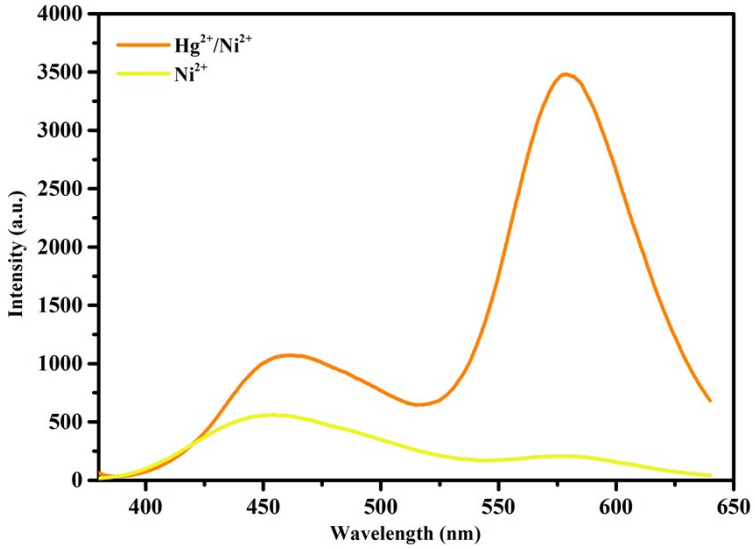

Figure S14. Luminescence intensity comparison of **1⊃DSM** upon addition of Hg^{2+} in the aqueous solution of Ni^{2+} ion. The concentration of Hg^{2+} and Ni^{2+} ions is 1×10^{-3} and 5×10^{-2} mol L^{-1}.

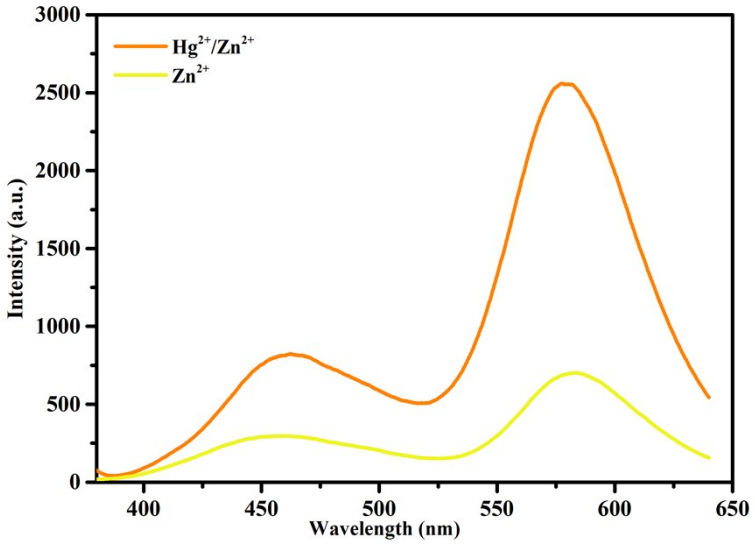

Figure S15. Luminescence intensity comparison of **1⊃DSM** upon addition of Hg^{2+} in the aqueous solution of Zn^{2+} ion. The concentration of Hg^{2+} and Zn^{2+} ions is 1×10^{-3} and 5×10^{-2} mol L^{-1}.

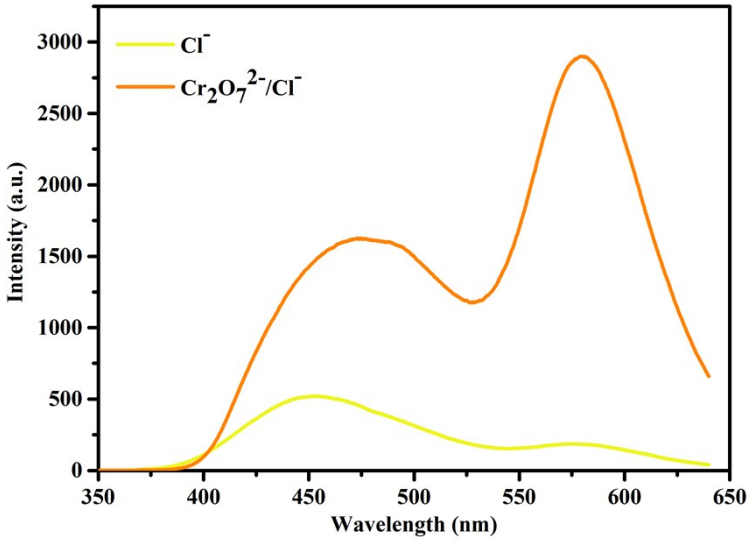

Figure S16. Luminescence intensity comparison of **1⊃DSM** upon addition of $Cr_2O_7^{2-}$ in the aqueous solution of Cl^- ion. The concentration of $Cr_2O_7^{2-}$ and Cl^- ions is 1×10^{-3} and 5×10^{-2} mol L^{-1}.

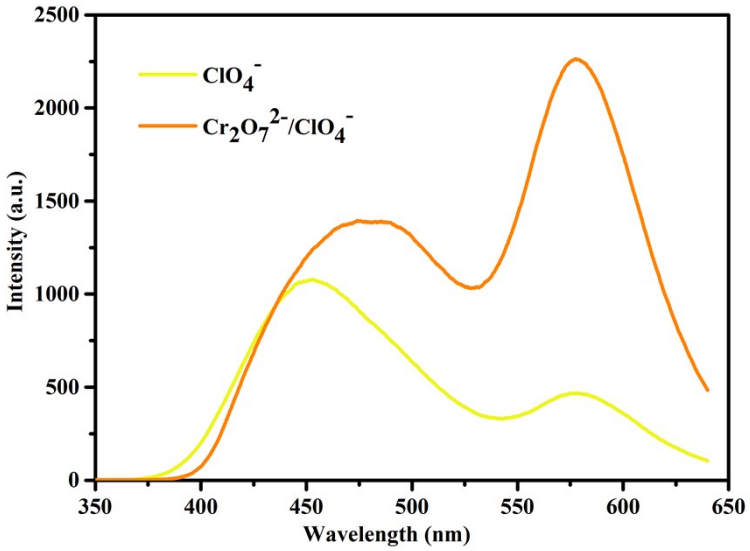

Figure S17. Luminescence intensity comparison of **1⊃DSM** upon addition of $Cr_2O_7^{2-}$ in the aqueous solution of ClO_4^- ion. The concentration of $Cr_2O_7^{2-}$ and ClO_4^- ions is 1×10^{-3} and 5×10^{-2} mol L^{-1}.

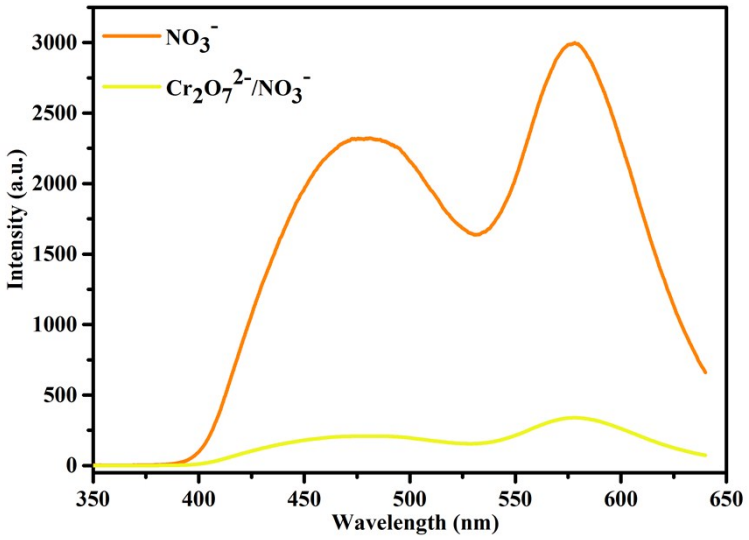

Figure S18. Luminescence intensity comparison of **1⊃DSM** upon addition of $Cr_2O_7^{2-}$ in the aqueous solution of NO_3^- ion. The concentration of $Cr_2O_7^{2-}$ and NO_3^- ions is 1×10^{-3} and 5×10^{-2} mol L^{-1}.

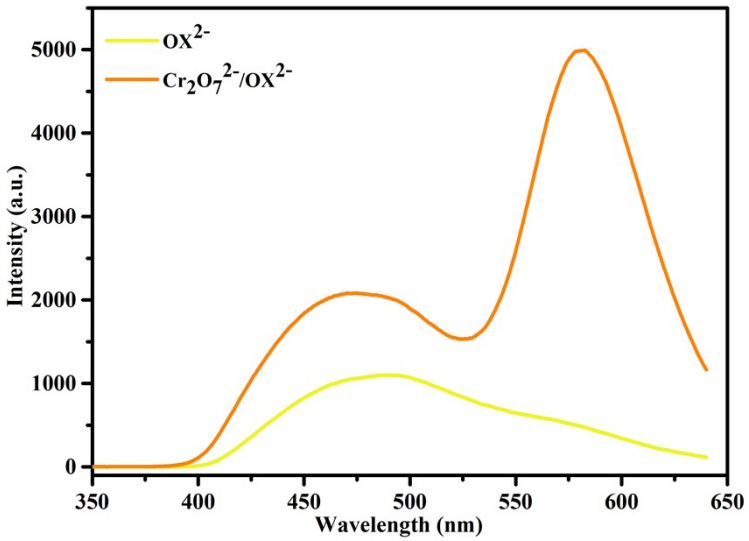

Figure S19. Luminescence intensity comparison of **1⊃DSM** upon addition of $Cr_2O_7^{2-}$ in the aqueous solution of ox^{2+} ion. The concentration of $Cr_2O_7^{2-}$ and ox^{2-} ions is 1×10^{-3} and 5×10^{-2} mol L^{-1}.

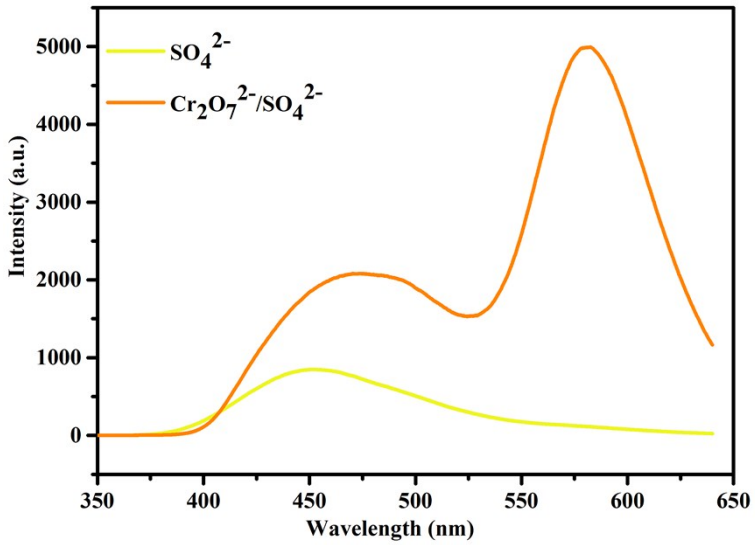

Figure S20. Luminescence intensity comparison of **1⊃DSM** upon addition of $Cr_2O_7^{2-}$ in the aqueous solution of SO_4^{2-} ion. The concentration of $Cr_2O_7^{2-}$ and SO_4^{2-} ions is 1 × 10^{-3} and 5 × 10^{-2} mol L^{-1}.

3.2 The sensing of the nitro explosives in aqueous solution

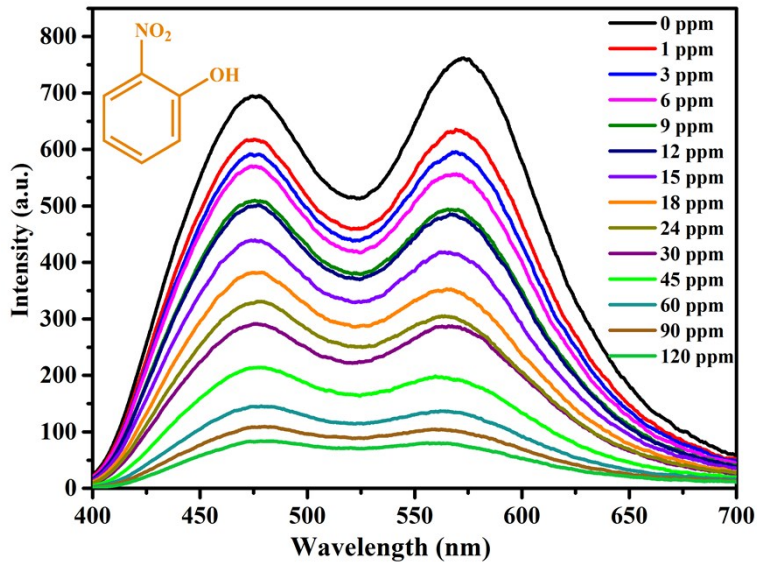

Figure S21. Fluorescence emission profile **1⊃DSM** towards 2-NP through the gradual addition of 2-NP aqueous solution.

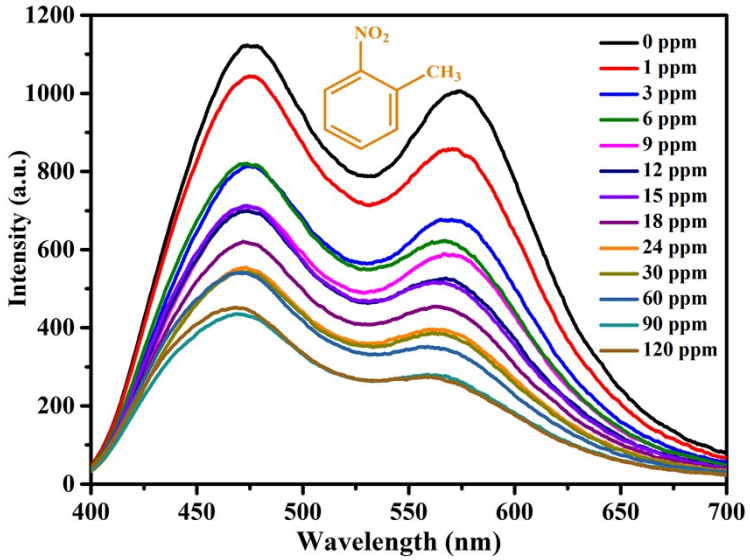

Figure S22. Fluorescence emission profile **1⊃DSM** towards 2-NT through the gradual addition of 2-NT aqueous solution.

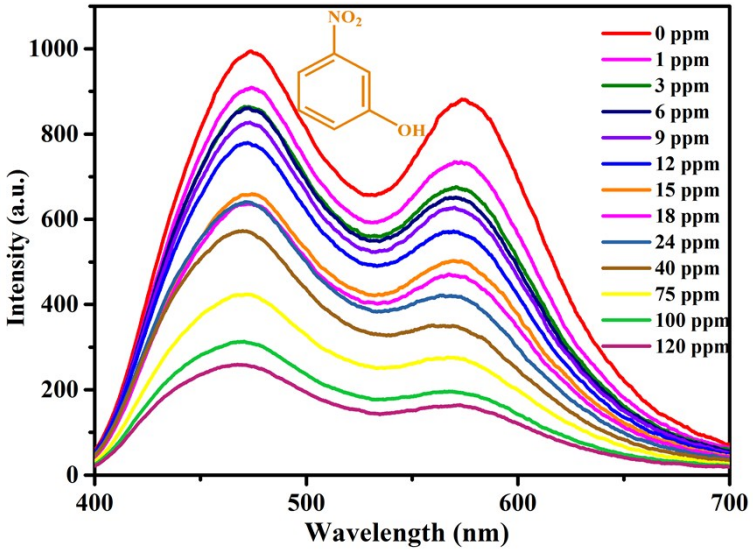

Figure S23. Fluorescence emission profile **1⊃DSM** towards 3-NP through the gradual addition of 3-NP aqueous solution.

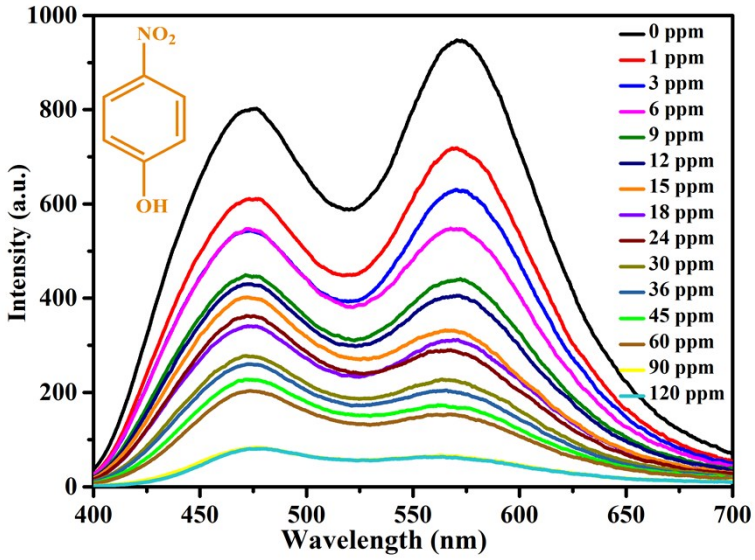

Figure S24. Fluorescence emission profile **1⊃DSM** towards 4-NP through the gradual addition of 4-NP aqueous solution.

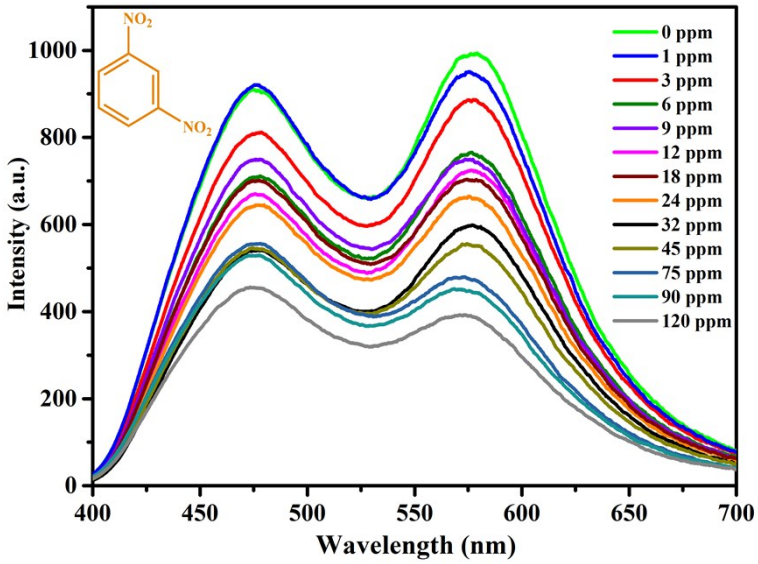

Figure S25. Fluorescence emission profile **1⊃DSM** towards 1,3-DNB through the gradual addition of 1,3-DNB aqueous solution.

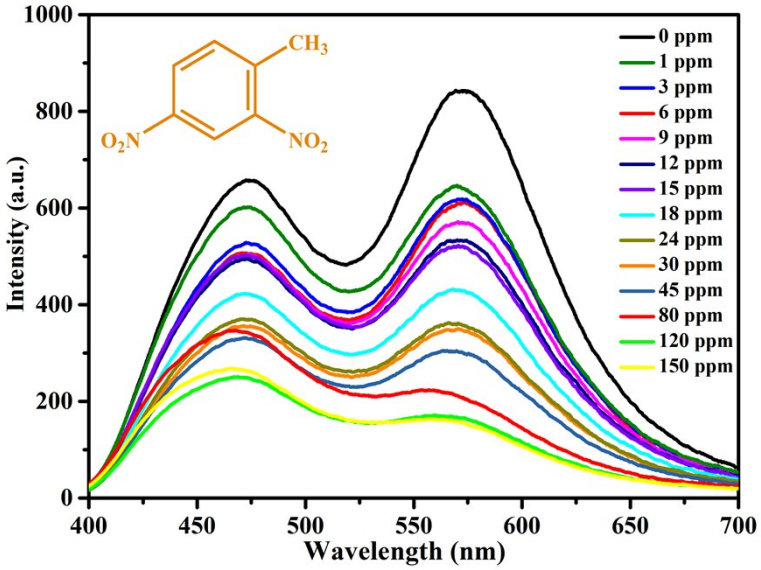

Figure S26. Fluorescence emission profile **1⊃DSM** towards 2,4-DNT through the gradual addition of 2,4-DNT aqueous solution.

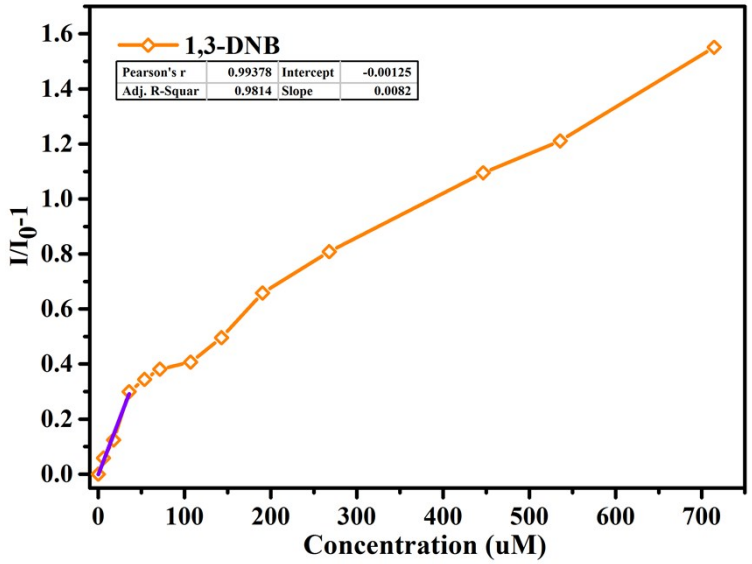

Figure S27. Concentration-dependent luminescence intensities by the addition of different contents of 1,3-DNB in aqueous solution, the red line is the linear fitting.

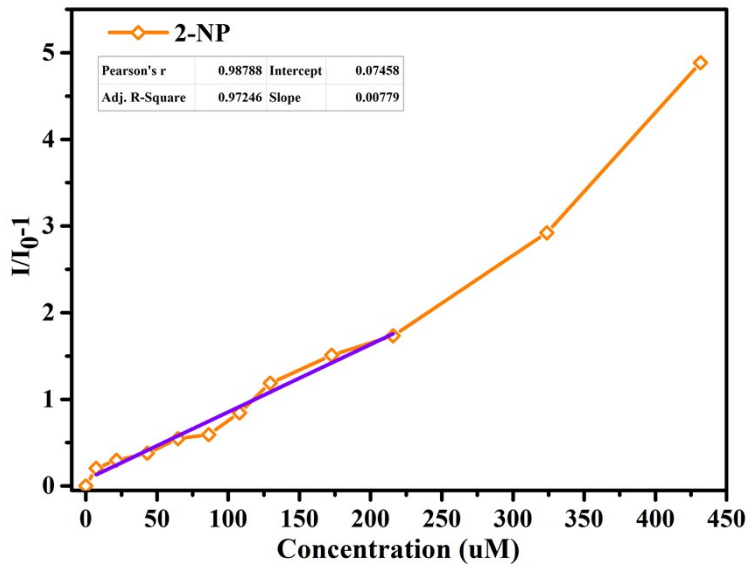

Figure S28. Concentration-dependent luminescence intensities by the addition of different contents of 2-NP in aqueous solution, the purple line is the linear fitting.

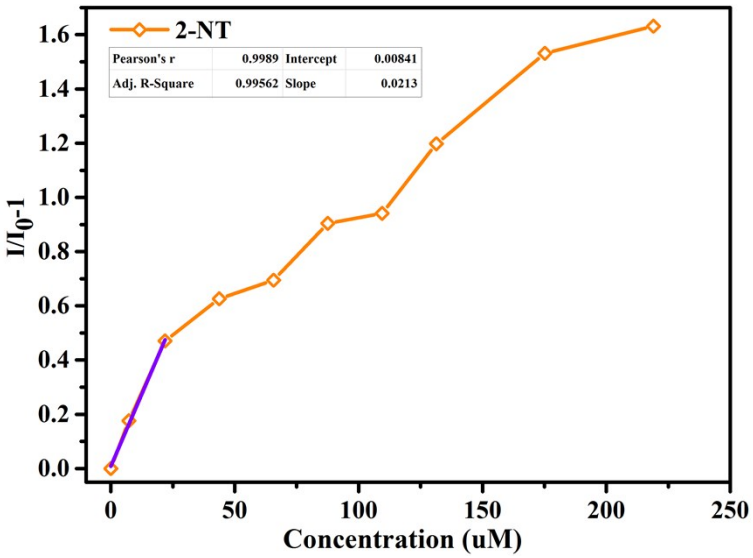

Figure S29. Concentration-dependent luminescence intensities by the addition of different contents of 2-NT in aqueous solution, the purple line is the linear fitting.

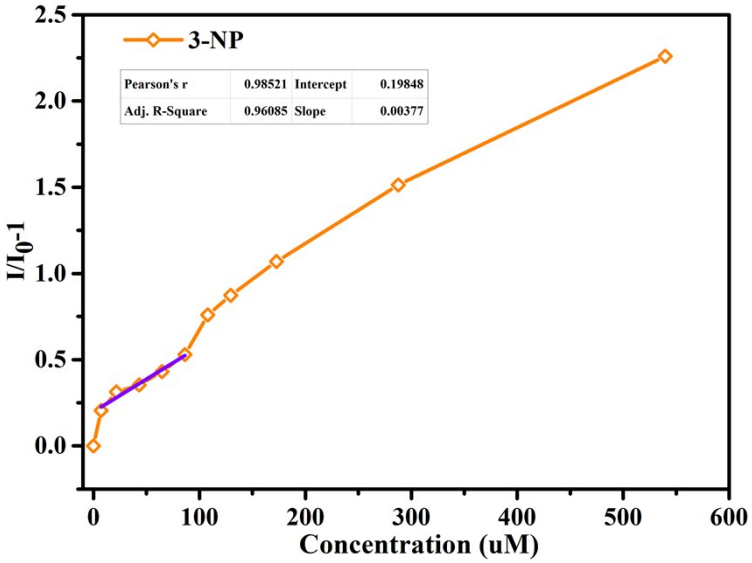

Figure S30. Concentration-dependent luminescence intensities by the addition of different contents of 3-NP in aqueous solution, the purple line is the linear fitting.

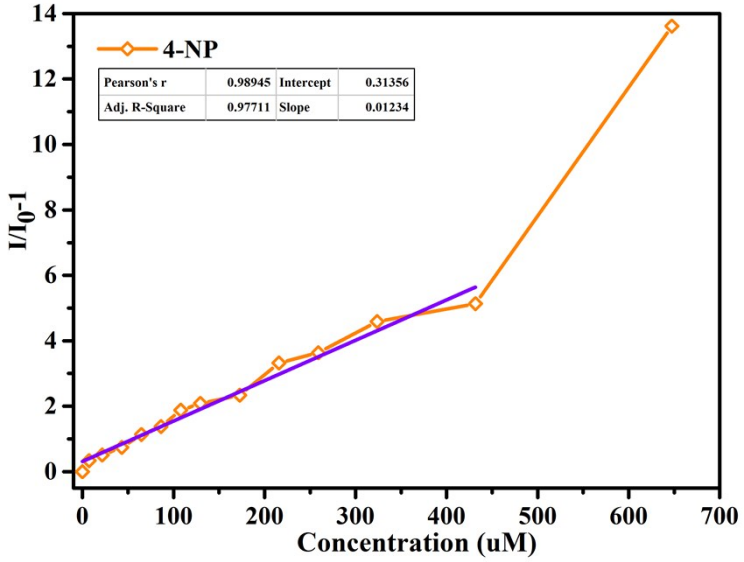

Figure S31. Concentration-dependent luminescence intensities by the addition of different contents of 4-NP in aqueous solution, the purple line is the linear fitting.

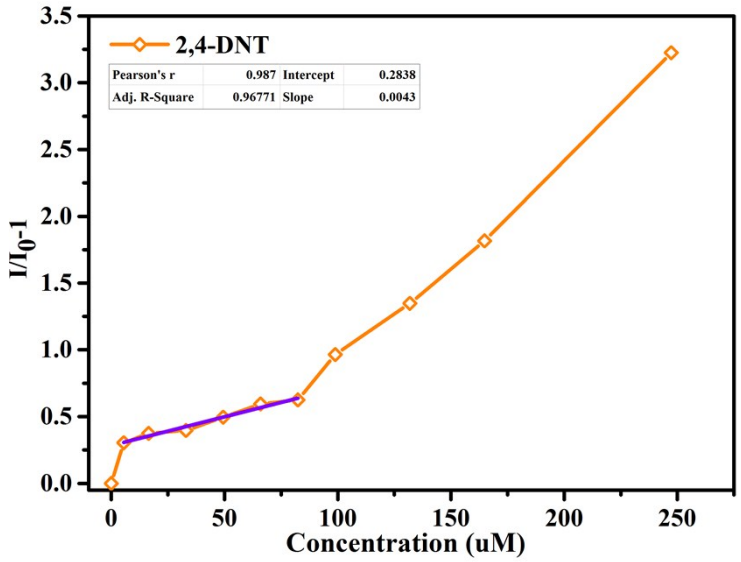

Figure S32. Concentration-dependent luminescence intensities by the addition of different contents of 2,4-DNT in aqueous solution, the purple line is the linear fitting.

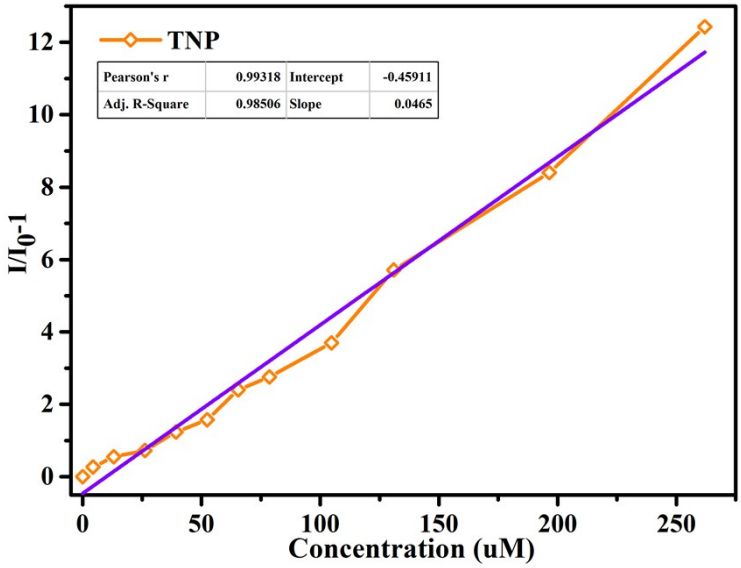

Figure S33. Concentration-dependent luminescence intensities by the addition of different contents of TNP in aqueous solution, the purple line is the linear fitting.

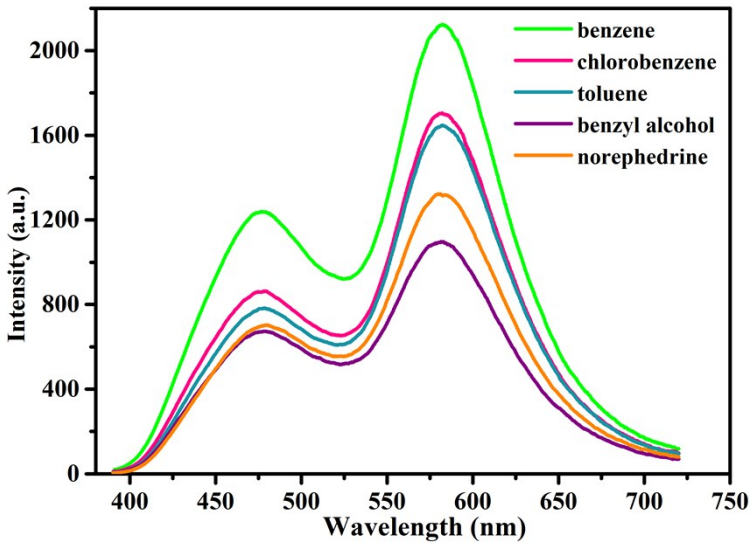

Figure S34. Fluorescence emission profile **1⊃DSM** towards other aromatics compounds without nitro groups, such as chlorobenzene, phenol, toluene, benzyl alcohol, norephedrine. The solution is the aqueous solution of analytes at 200 ppm for norephedrine and 0.2 mL/2mL (0.2 mL, the volume of pure solvent chlorobenzene, phenol, toluene, benzyl alcohol; 2 mL, the volume of the water solution; meanwhile, in order to add the solubility of aromatics compounds, in fact, 0.2 mL solvent is ethanol of chlorobenzene, phenol, toluene, benzyl alcohol) for other four aromatics compounds.

3.3 The vapor-phase sensing of 1⊃DSM towards nitro explosives

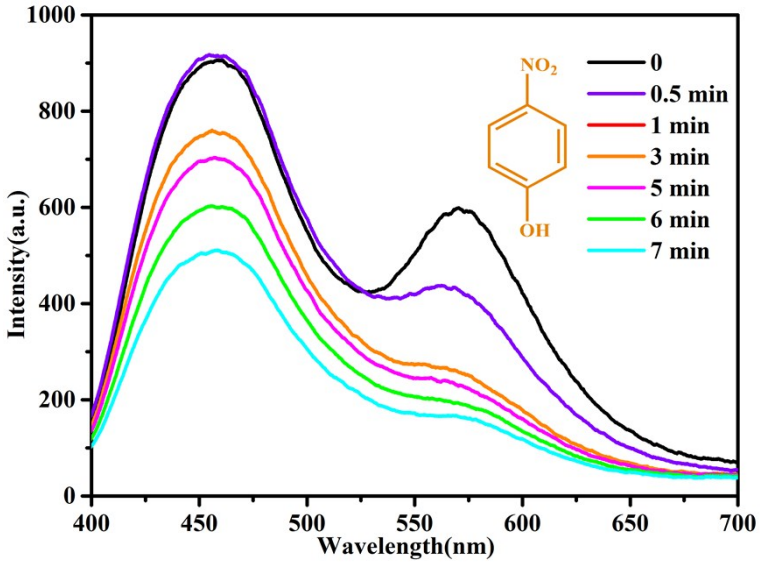

Figure S35. Fluorescence emission profile **1⊃DSM** exposure to 4-NP.

3.4 The sensing of the nitro-containing antibiotics in aqueous solution

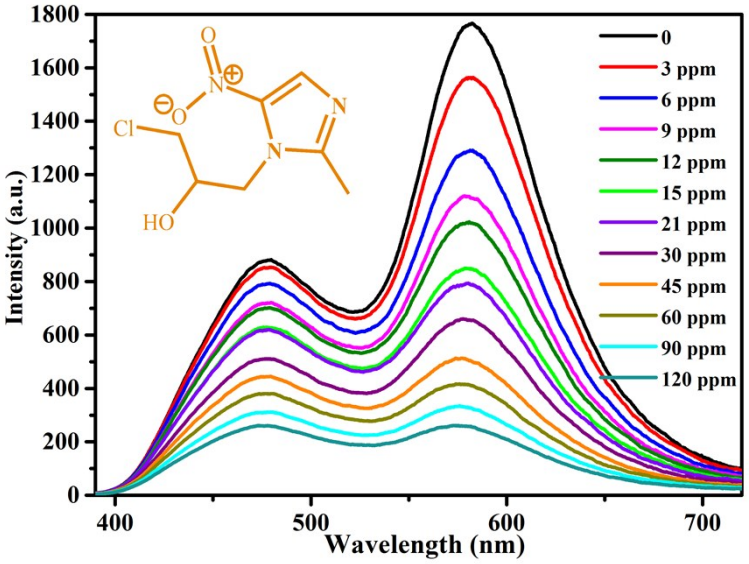

Figure S36. Fluorescence emission profile **1⊃DSM** towards ODT through the gradual addition of ODT aqueous solution.

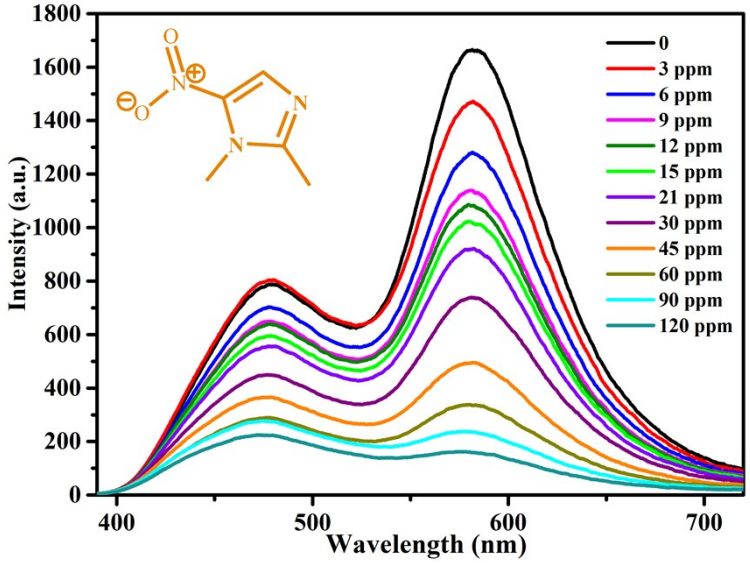

Figure S37. Fluorescence emission profile **1⊃DSM** towards DTZ through the gradual addition of DTZ aqueous solution.

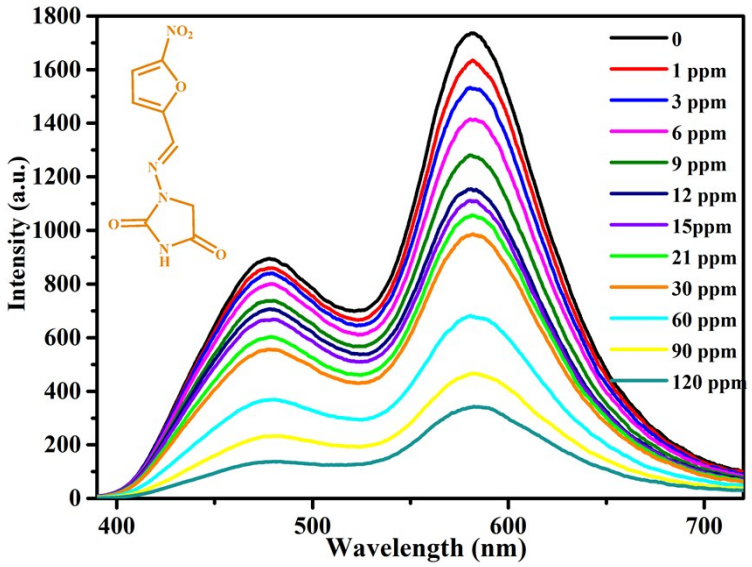

Figure S38. Fluorescence emission profile **1⊃DSM** towards NFT through the gradual addition of NFT aqueous solution.

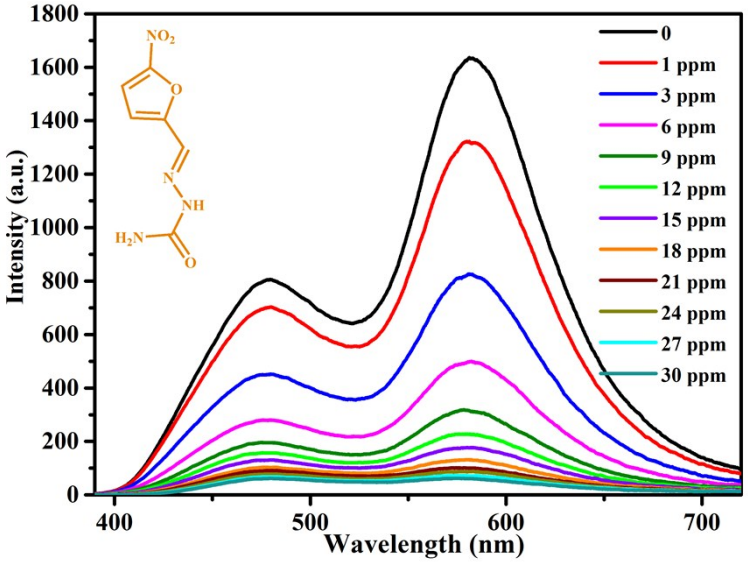

Figure S39. Fluorescence emission profile **1⊃DSM** towards NZF through the gradual addition of NZF aqueous solution.

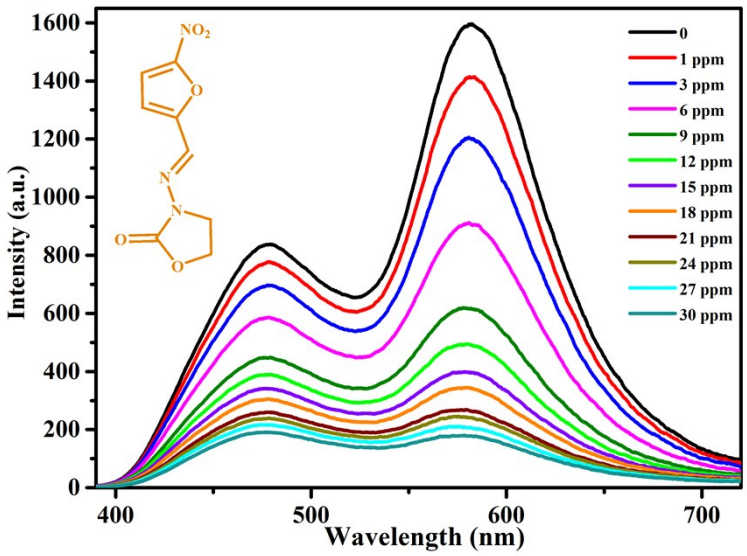

Figure S40. Fluorescence emission profile **1⊃DSM** towards FZD through the gradual addition of FZD aqueous solution.

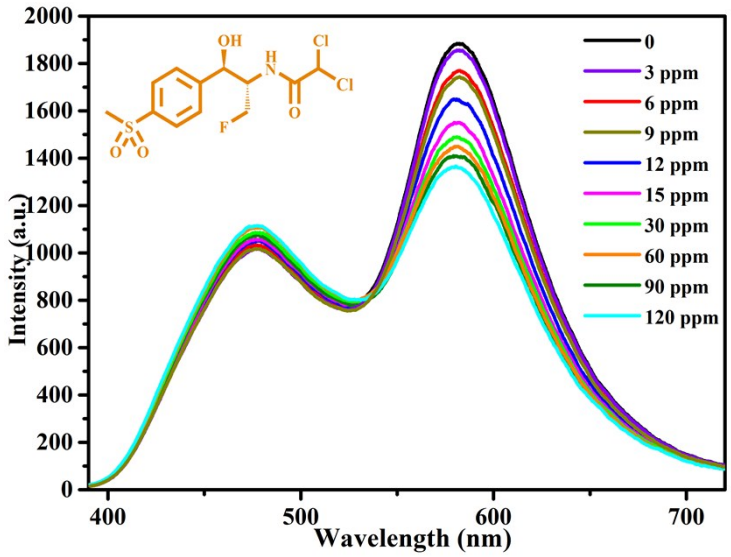

Figure S41. Fluorescence emission profile **1⊃DSM** towards FFC through the gradual addition of FFC aqueous solution.

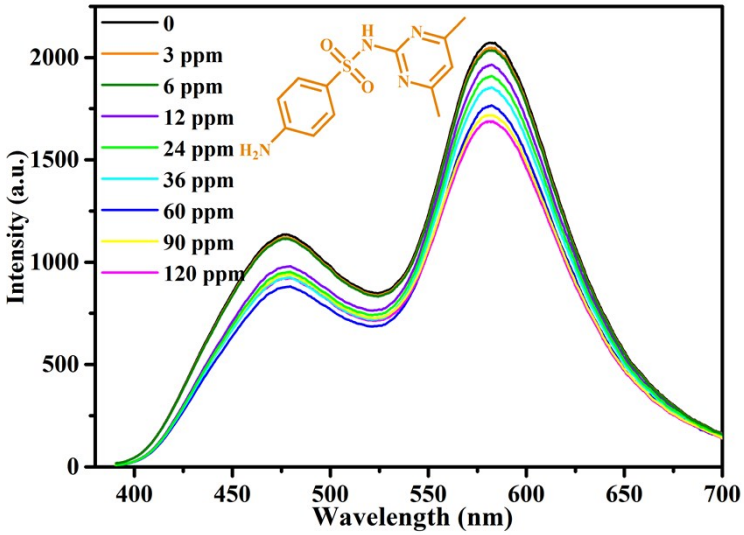

Figure S42. Fluorescence emission profile **1⊃DSM** towards SMZ through the gradual addition of SMZ aqueous solution.

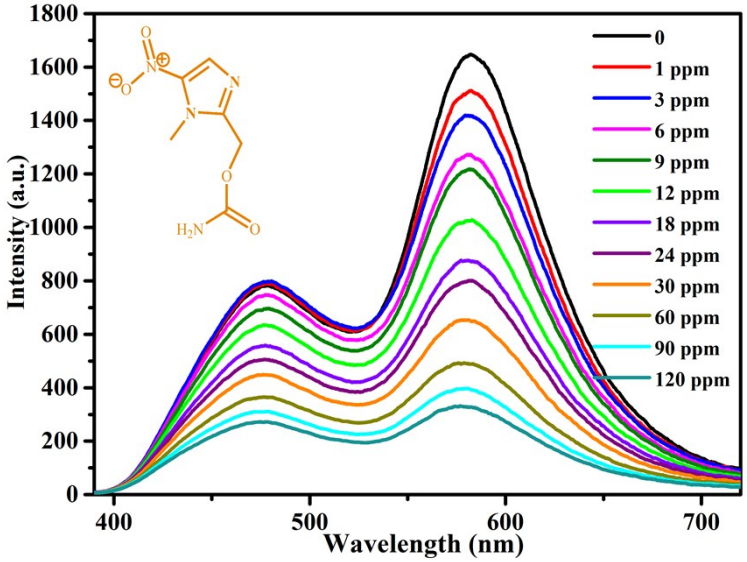

Figure S43. Fluorescence emission profile **1⊃DSM** towards RDZ through the gradual addition of RDZ aqueous solution.

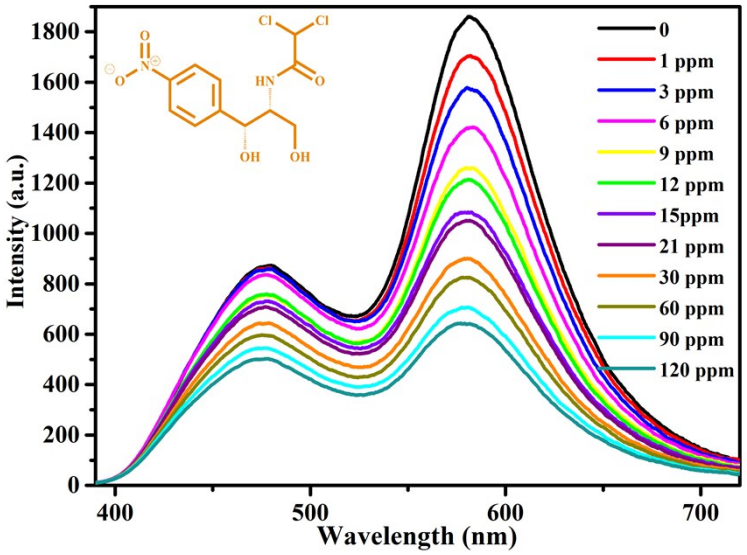

Figure S44. Fluorescence emission profile **1⊃DSM** towards CAP through the gradual addition of CAP aqueous solution.

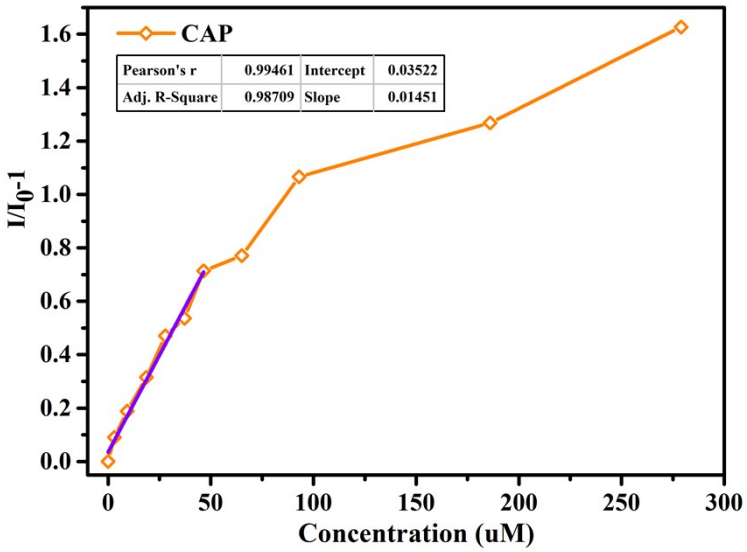

Figure S45. Concentration-dependent luminescence intensities by the addition of different contents of CAP in aqueous solution, the purple line is the linear fitting.

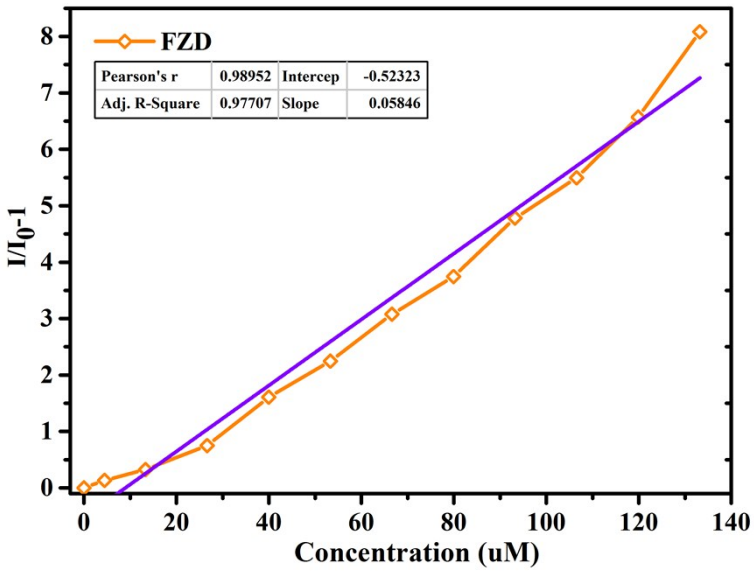

Figure S46. Concentration-dependent luminescence intensities by the addition of different contents of FZD in aqueous solution, the purple line is the linear fitting.

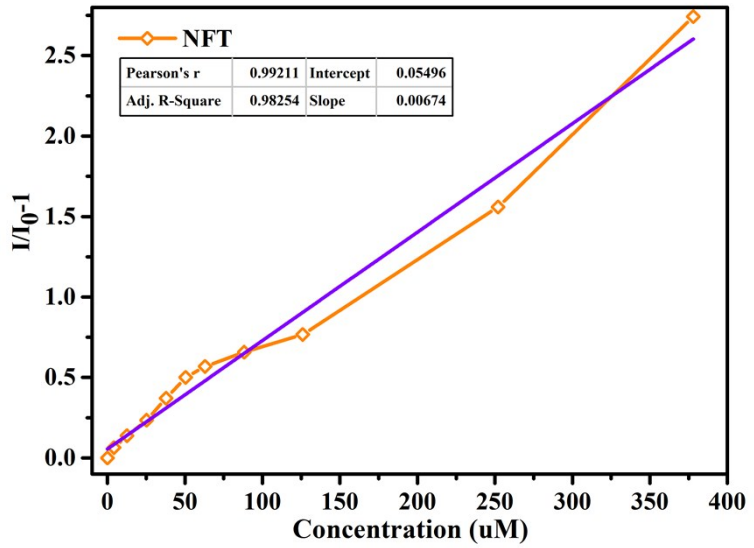

Figure S47. Concentration-dependent luminescence intensities by the addition of different contents of NFT in aqueous solution, the purple line is the linear fitting.

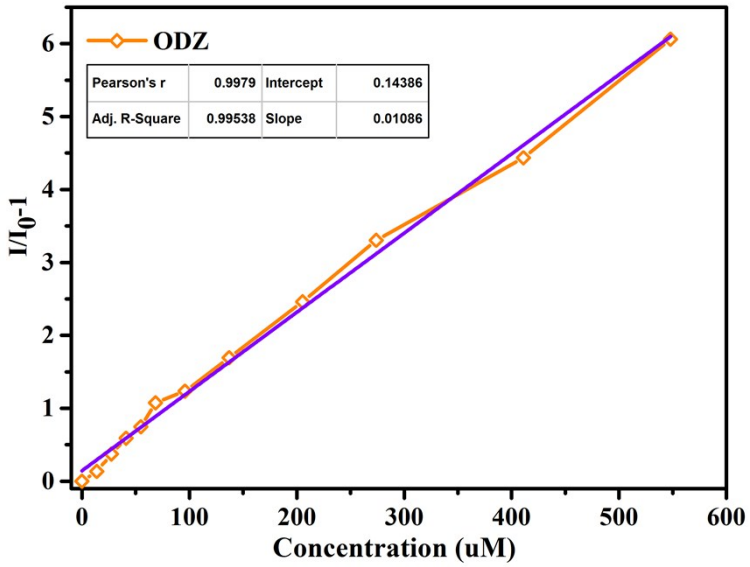

Figure S48. Concentration-dependent luminescence intensities by the addition of different contents of ODT in aqueous solution, the purple line is the linear fitting.

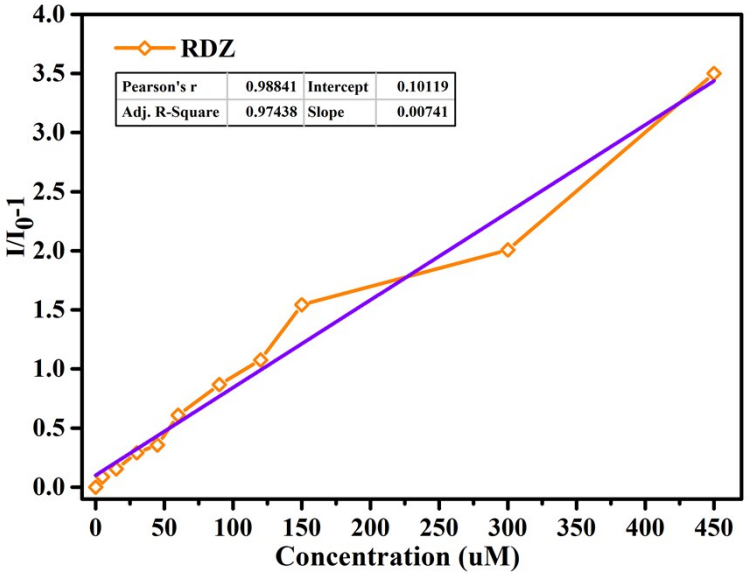

Figure S49. Concentration-dependent luminescence intensities by the addition of different contents of RDZ in aqueous solution, the purple line is the linear fitting.

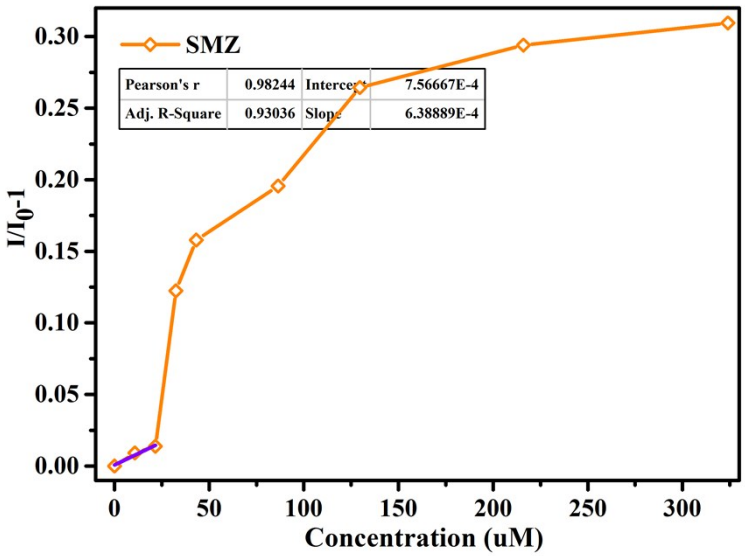

Figure S50. Concentration-dependent luminescence intensities by the addition of different contents of SMZ in aqueous solution, the purple line is the linear fitting.

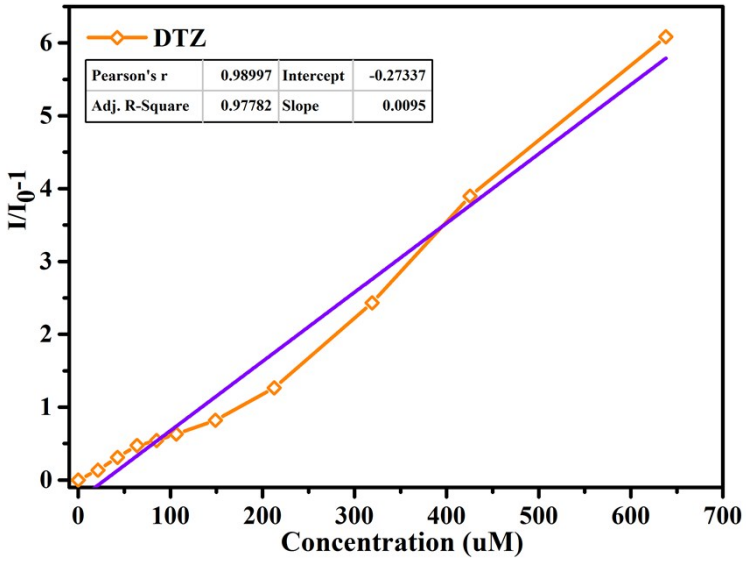

Figure S51. Concentration-dependent luminescence intensities by the addition of different contents of DTZ in aqueous solution, the purple line is the linear fitting.

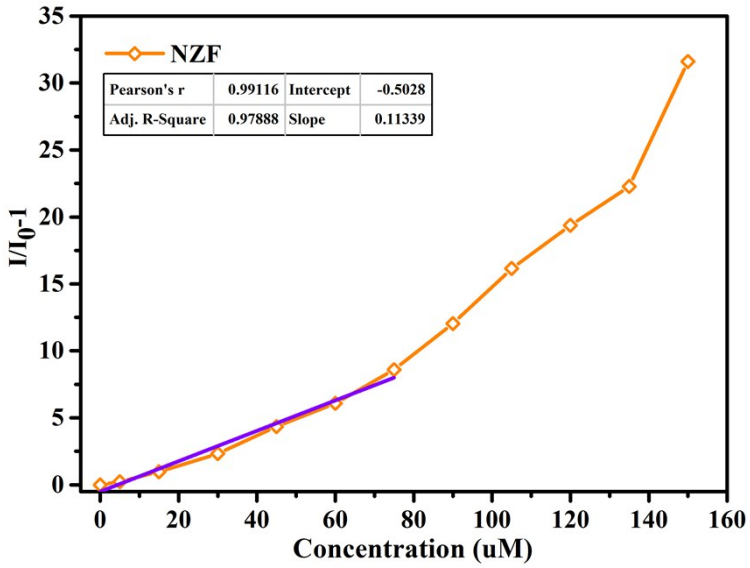

Figure S52. Concentration-dependent luminescence intensities by the addition of different contents of NZF in aqueous solution, the purple line is the linear fitting.

5. The UV-vis spectera

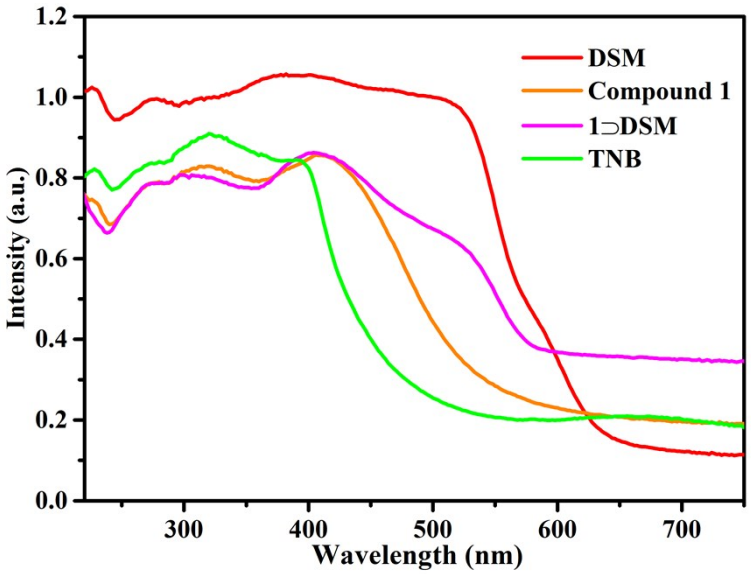

Figure S53. UV-vis absorption spectrum of TNB, DSM, compound **1** and **1⊃DSM** in solid state.

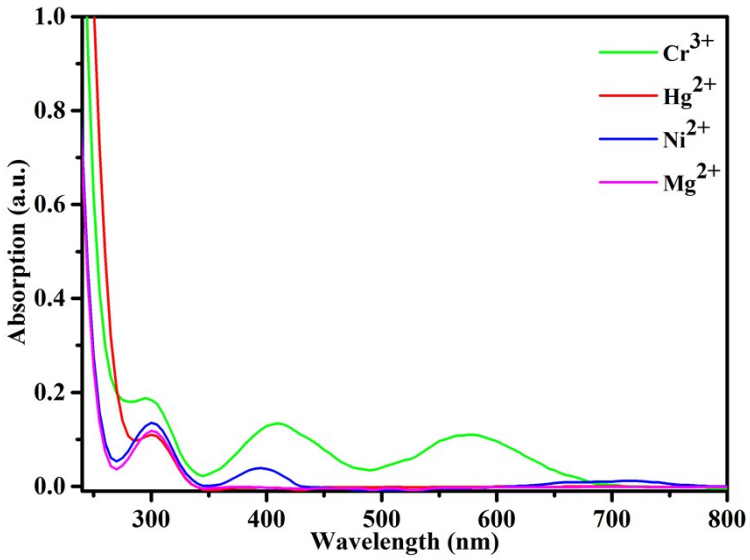

Figure S54. UV-vis absorption spectrum of Cr^{3+}, Hg^{2+}, Ni^{2+}, Mg^{2+} in aqueous solution. The concentration of each ion is 1×10^{-4} mol L^{-1}.

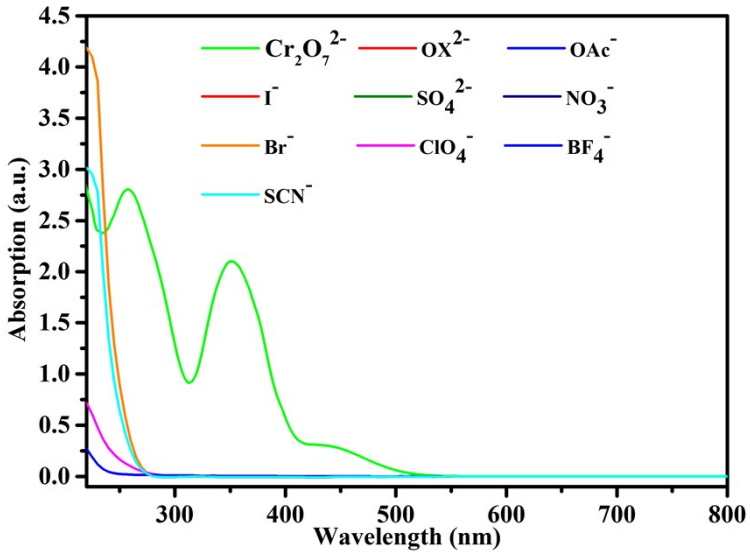

Figure S55. UV-vis absorption spectrum of various anions in aqueous solution. The concentration of each ion is 1×10^{-4} mol L^{-1}.

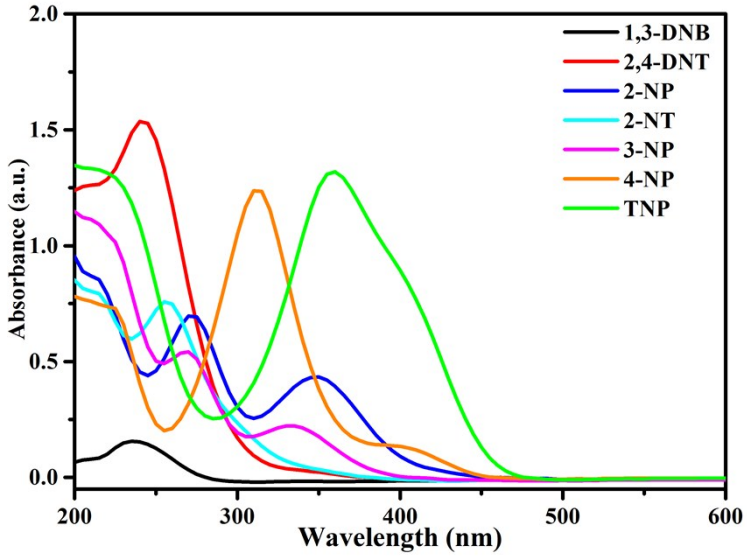

Figure S56. UV-vis absorption spectrum of nitro explosives in aqueous solution.

6. The calculations of the HOMOs and LUMOs of the nitro-explosives

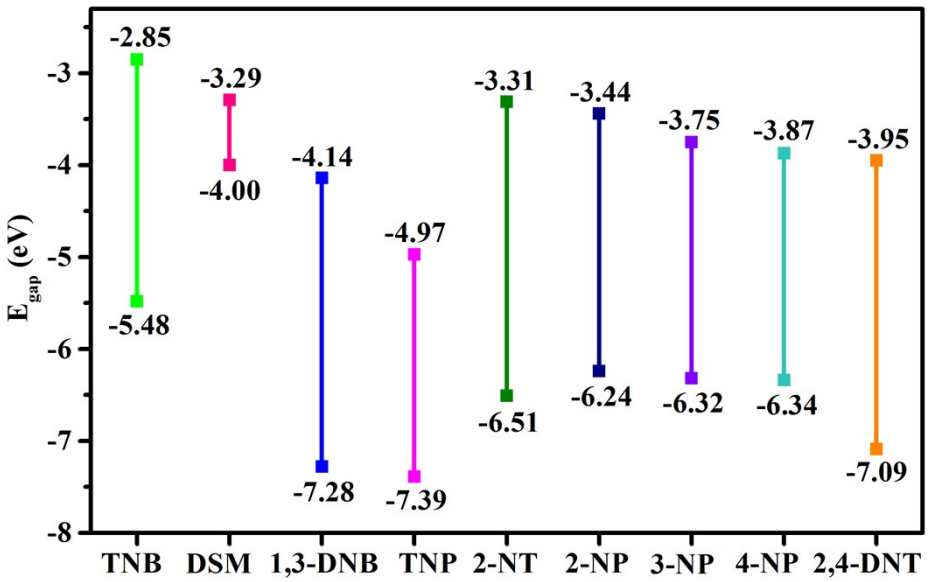

Figure S57. The calculations of the HOMOs and LUMOs of the nitro-explosives.

7. Powder X-ray Diffraction Studies

X-ray powder diffraction (XPD) patterns of **1** was collected on a D/Max-2500 diffractometer using Cu-*K*α (λ = 1.5418 Å) beam at room temperature.

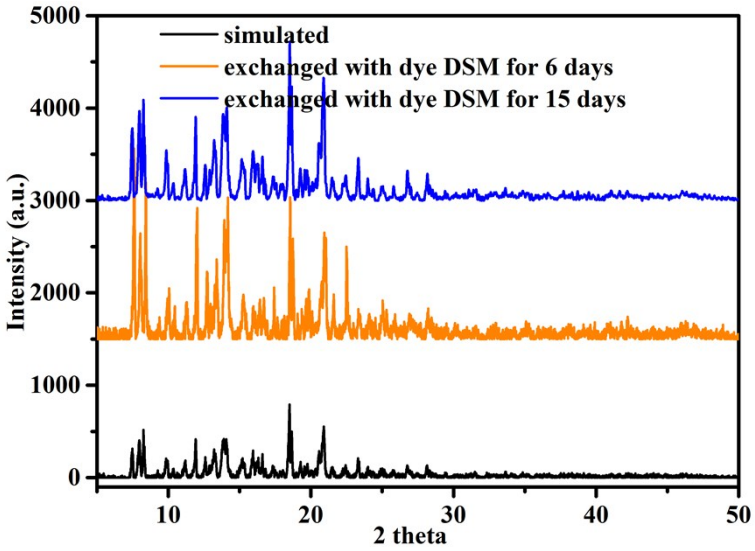

Figure S58. PXRD patterns of as-synthesized **1** as well as samples **1⊃DSM** which was soaked in the DMF solution for 6 and 15 days.

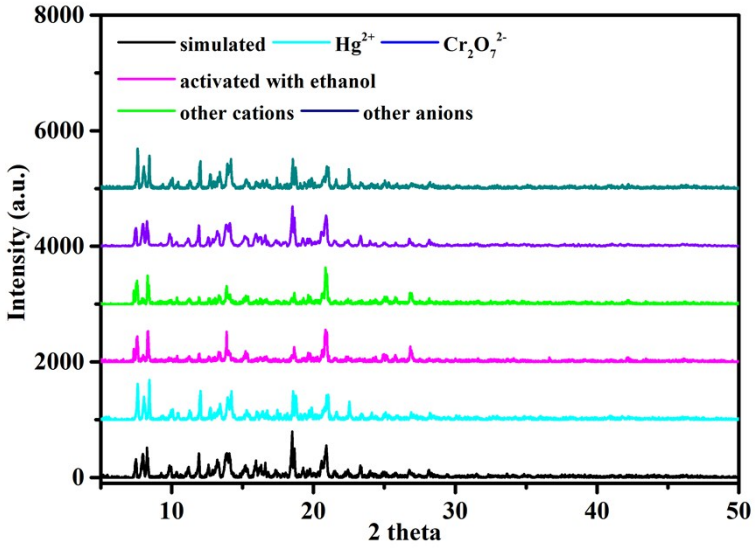

Figure S59. PXRD patterns of **1⊃DSM** after fluorescence sensing in 1×10^{-3} mol L^{-1} aqueous solution of Hg^{2+} and other cations, PXRD patterns of **1⊃DSM** in 1×10^{-3} mol L^{-1} aqueous solution of $Cr_2O_7^{2-}$ and other anions. Other cations: the mixed aqueous solution of other cations (the concentration of each cation is 1×10^{-3} mol L^{-1}). Other anions: the mixed aqueous solution of other cations (the concentration of each anion is 1×10^{-3} mol L^{-1}).

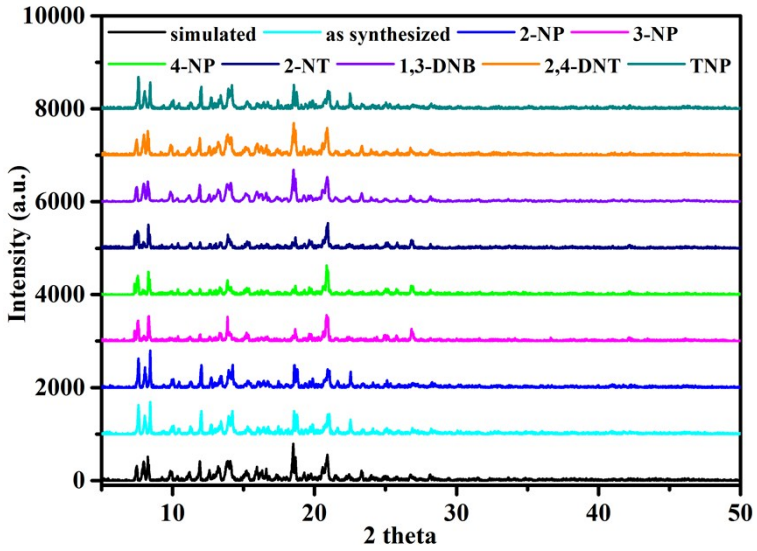

Figure S60. PXRD patterns of **1⊃DSM** after fluorescence sensing in the aqueous solutions of the various nitro explosives (the concentration of each species is 300 ppm).

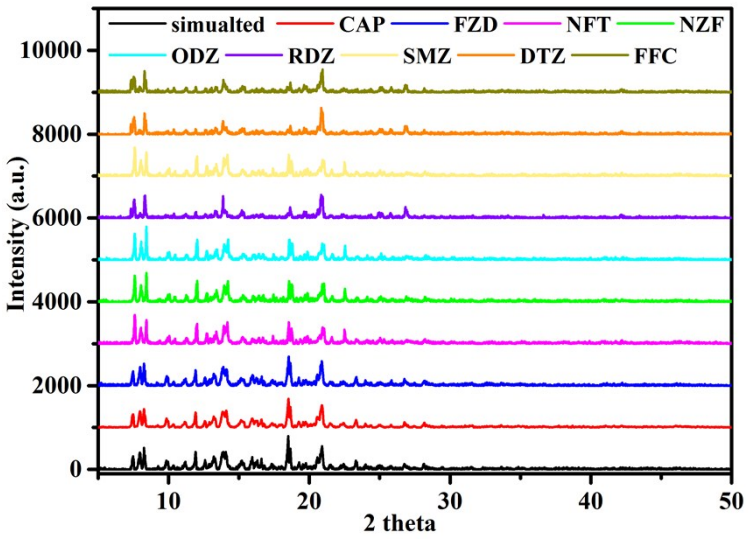

Figure S61. PXRD patterns of **1⊃DSM** after fluorescence sensing in the aqueous solutions of the various nitro-containing antibiotics (the concentration of each species is 200 ppm).

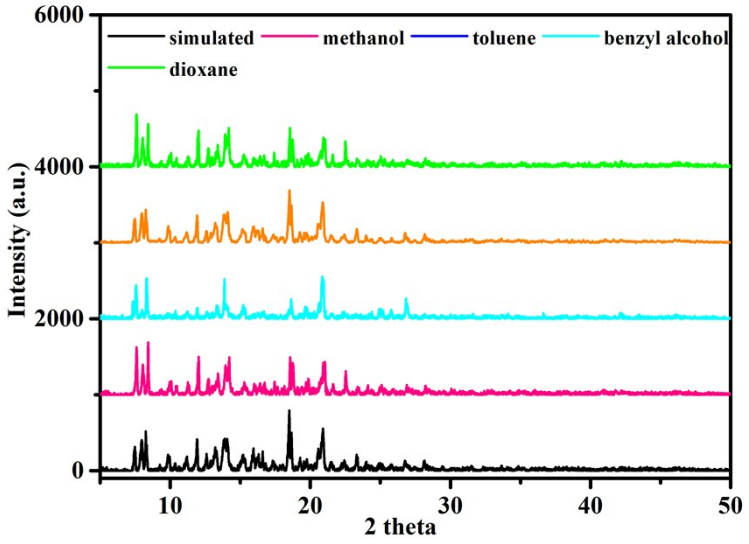

Figure S62. PXRD patterns of **1⊃DSM** after fluorescence sensing in the various solvents.

8. Themogravimetric Analysis of MOFs

Thermal Gravimetric Analysis (TGA) was carried out using a Netszch TGA 209 F3 simultaneous TG thermoanalyzer, under an air atmosphere in the range of 30 to 800 °C and at a heating rate of 5 °C min^{-1}.

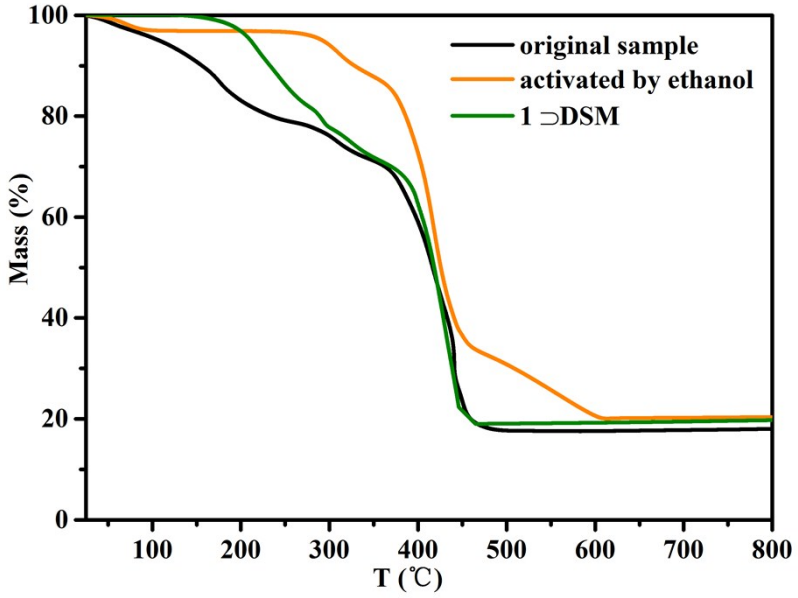

Figure S63. TGA curves of compound **1** and **1⊃DSM** under air atmosphere.

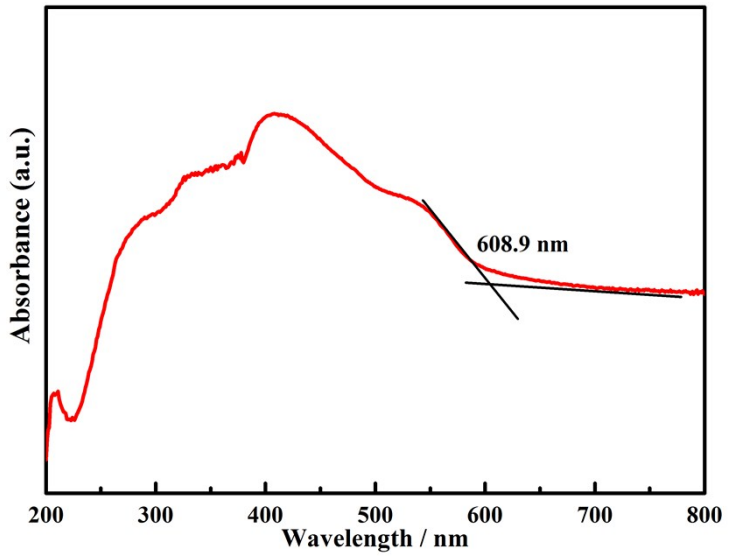

Figure S64. Solid ultraviolet diffraction reflectance spectra of **1⊃DSM.**

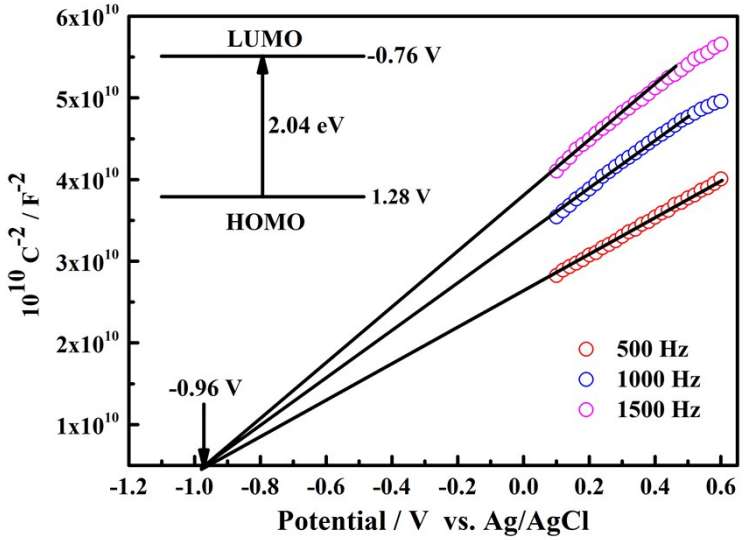

Figure S65. The Mott–Schottky spectra and energy band position of **1⊃DSM.**